Mesenchyme governs hair follicle induction

Otto J.M. Mäkelä[1] and Marja L. Mikkola[1]

[1]Cell and Tissue Dynamics Research Program, Institute of Biotechnology, Helsinki Institute of Life Sciences (HiLIFE), University of Helsinki, Finland

Corresponding author: Marja L. Mikkola (marja.mikkola@helsinki.fi)

Keywords: hair follicle, induction, embryonic development, tissue recombination, R-spondin, Bmp

Abstract

Tissue interactions are essential to guide organogenesis. The development of hair follicles is regulated by inductive signalling between the embryonic surface epithelium and the adjacent mesenchyme. Previous studies have established that the mesenchymal component of the hair follicle, the dermal papilla and its precursor dermal condensate, has the capacity for de novo hair follicle induction. However, studies prior to dermal condensate formation have been inconclusive, and therefore the source and the identity of the primary inductive signal have remained unknown. Here, we performed epithelial-mesenchymal tissue recombination experiments using hair-forming back skin and glabrous plantar skin from mouse embryos to unveil that the back skin mesenchyme is inductive even prior to dermal condensate formation. Moreover, the naïve, unpatterned mesenchyme was sufficient to trigger hair follicle formation even in the oral epithelium. Considering the recognized role of Wnt signalling and Bmp activity inhibition in initiation of hair follicle development, we explored the hair-inductive ability of the Wnt agonist R-spondin-1 and a Bmp receptor inhibitor in embryonic skin explants. Although R-spondin-1 instigated precocious placode-specific transcriptional responses, it alone or in combination with the Bmp receptor inhibitor was insufficient for hair follicle induction. Our findings pave the way for identifying the hair follicle-inducing cue.

Introduction

Inductive tissue interactions constitute a fundamental mechanism regulating embryonic development. As most organs develop from multiple tissue types, cell-cell communication across tissue boundaries is critical to ensure successful organ induction, patterning, morphogenesis, and cell differentiation (Thesleff, Vaahtokari & Partanen, 1995). The hair follicle is an excellent model to study these interactions as it develops from the embryonic surface ectoderm and the underlying mesenchyme, and reciprocal signalling between these compartments directs its development, as well as the life-long cyclic function of the mature organ (Hardy, 1992; Sennett & Rendl, 2012; Morgan, 2014; Li & Tumbar, 2021). The inductive signalling regulating hair follicle development and renewal has been under meticulous investigation for decades, yet some key aspects remain elusive to date.

In mice, hair follicles are induced in three consecutive waves, the first one commencing around embryonic day E13.5 (Fliniaux et al., 2008; Biggs et al., 2018) as a response to a yet unidentified primary inductive signal. As a result, epithelial keratinocytes migrate centripetally to form a

thickening, the placode (Ahtiainen et al., 2014). Inductive signals from the placode then induce the underlying fibroblasts to migrate and aggregate underneath the placode, forming the mesenchymal component of the hair follicle, the dermal condensate (DC) (Glover et al., 2017; Biggs et al., 2018; Gupta et al., 2019; Mok et al., 2019). Subsequently, secondary inductive signals from the DC promote invagination of the epithelium to the mesenchyme, and the DC is engulfed by the epithelium and remains an integral part of the mature hair follicle, named the dermal papilla (DP) (Sennett & Rendl, 2012). As the embryo grows larger, secondary and tertiary hair placodes form between the existing hair primordia in two waves at around E16.5 and E18.5, respectively (Duverger & Morasso, 2009).

Tissue crosstalk between the follicular epithelium and the underlying mesenchyme is mediated by conserved signalling pathways (Biggs & Mikkola, 2014). Initially, Wnt/β-catenin signalling is focally activated in the prospective placode where it is necessary for placode formation as suppression of epithelial β-catenin signalling activity blocks hair placode formation altogether (Andl et al., 2002; Zhang et al., 2009; Huelsken et al., 2001). Moreover, forced activation of epithelial Wnt/β-catenin signalling is thus far the only known genetic manipulation to induce precocious formation of hair placodes (Närhi et al., 2008; Zhang et al., 2008). After initial epithelial Wnt activation, Eda/Edar/NF-κB pathway is necessary to reinforce Wnt activity and placode morphogenesis to continue (Schmidt-Ullrich et al., 2006; Fliniaux et al., 2008; Zhang et al., 2009). Once placode formation has initiated, signals emanating from the placode, in particular fibroblast growth factor 20 (Fgf20) and Sonic hedgehog (Shh), govern DC formation (Huh et al., 2013; Woo, Zhen & Oro, 2012). Fgf20 has been shown to induce directional migration of mesenchymal fibroblasts and to induce DC cell fate (Mok et al., 2019; Biggs et al., 2018). Fgf20 is necessary for DC formation, as demonstrated by the absence of all molecular and morphological indications of primary and secondary DCs in *Fgf20* null mice (Huh et al., 2013; Biggs et al., 2018; Mok et al., 2019).

Several lines of evidence indicate that suppression of Bmp signalling is essential for hair follicle induction. Deletion of Bmp-inhibitor gene *Noggin*, expressed in the DC, suppresses secondary and tertiary hair placode formation (Botchkarev et al., 1999, 2002), while its ectopic expression under the *Keratin 14* promoter results in increased hair follicle density and formation of ectopic hair follicles in ventral paws and at the site of the Meibomian glands (Plikus et al., 2004). Furthermore, Noggin-treatment increases hair placode density in embryonic skin explants, whereas Bmp4-treatment prevents hair placode formation by suppressing expression of *Edar* and *Lef1*, the mediator of Wnt/β-catenin pathway (Botchkarev et al., 1999; Mou et al., 2006; Jamora et al., 2003).

In the past, hair follicle induction has been studied extensively by transplantation and tissue recombination experiments. It was first demonstrated that the whisker follicle DP contains the capacity to induce new follicles by transplantation of rat vibrissae DPs in the ear skin and subsequent formation of ectopic whisker follicles (Cohen, 1961). Later, tissue recombination of hair-forming dorsal mesenchyme with the glabrous plantar epithelium revealed that the inductive capacity resides in the dorsal skin mesenchyme as early as the DC forms (Kollar, 1970). These and other studies have established that the hair follicle dermal component, the DP and its precursor the DC, contain the capacity to induce *de novo* hair follicle formation in the skin, as well as other epithelial tissue of ectodermal origin, such as dental and corneal epithelia (Oliver, 1970; Kollar, 1970; Hardy, 1992; Ferraris et al., 2000; Dhouailly, 1973; Cohen, 1961; Kollar & Baird, 1970; Higgins et al., 2013; Jahoda et al., 1992). The extrapolation of these findings has established the current paradigm, which posits that the mesenchyme is the site of the hair-inductive signal. However, experiments investigating the inductive capacity of the mesenchyme prior to DC formation are scarce. In fact, recombination of mouse back skin mesenchyme prior to hair follicle induction (E12.5) with glabrous epithelia of chick embryonic skin did not result in appendage induction (Dhouailly, 1973). In contrast, the reverse recombination of the E12.5 hair-forming back skin epithelium with the glabrous chick skin mesenchyme produced short epithelial nodules protruding into the dermis (Dhouailly, 1973). Furthermore, studies showing that DC formation is preceded by a placodal prepattern (Huh et al., 2013; Glover et al., 2017; Biggs et al., 2018; Mok et al., 2019) and that primary and secondary hair placodes form in the absence of DCs in *Fgf20* null embryos (Huh et al., 2013) have challenged the prevailing model of mesenchymal induction of hair follicle formation.

Here, we sought to identify the source of the hair follicle inductive cue by performing tissue recombination experiments between heterologous epithelia and mesenchymes using genetically labelled tissues expressing fluorescent reporters allowing unambiguous assessment of tissue purity. Our results reveal that the hair follicle inductive signals reside in the mesenchyme even prior to DC formation. We show that mesenchymal expression of the Wnt pathway agonist *R-spondin-1 (Rspo1*) is upregulated at the time of hair follicle induction. This prompted us to assess the impact of Rspo1 on hair follicle induction in *ex vivo* cultured skin explants. Our results indicate that Rspo1 alone, or in combination with inhibition of Bmp-signalling, is insufficient to induce precocious hair follicle formation, although the latter altered hair placode patterning and the former instigated hair placode-specific transcriptional responses even prior to hair follicle induction. We expect our results will motivate further research to identify the mesenchymal hair-inductive cues.

105 **Results**

106 **Hair follicle inductive potential resides in the mesenchyme even prior to dermal condensate**
107 **formation**

108 To determine whether the hair follicle inductive signal arises from the epithelium or the
109 mesenchyme, we performed heterotypic tissue recombination between the hair-forming back skin
110 and the glabrous plantar skin by enzymatically separating the tissue compartments, recombining
111 them, and culturing *ex vivo*. To monitor the tissue separation efficiency and retrospectively verify
112 the origin of the cells, we collected epithelia from R26R$^{mTmG/+}$ and mesenchymes from R26R$^{mG/+}$
113 littermate embryos, ubiquitously expressing membrane-bound tdTomato (mT) and membrane-
114 bound eGFP (mG), respectively. Alternatively, epithelia were obtained from R26R$^{floxedTomato/+}$, or
115 R26R$^{floxedTomato/+}$;K17-GFP and mesenchymes from wild type embryos. First, we performed
116 homotypic recombinations of E14.5 tissues that served as technical controls. Dorsal skin
117 mesenchyme and epithelium cultured for 4 days readily formed hair follicle-like appendages,
118 whereas homotypic recombinants of plantar tissues did not generate any appendages (Fig. 1A)
119 validating our experimental set-up. In heterotypic recombinants, the DC-containing dorsal
120 mesenchymal tissue induced hair follicle-like appendage formation in the glabrous plantar
121 epithelium (Fig. 1A), as expected. No appendages were observed in the recombinants consisting of
122 dorsal skin epithelium and plantar mesenchyme (Fig. 1A).

123 We then asked where the inductive potential resides at the time of hair placode induction at E13.5,
124 when DCs cannot yet be morphologically discerned. Like E14.5 tissues, homotypic recombinations
125 between back skin epithelium and mesenchyme readily produced skin appendages, whereas
126 recombinations between plantar skin compartments did not (Fig. 1B). Interestingly, at this stage too,
127 hair follicle-like appendages were induced upon heterotypic recombination of the dorsal
128 mesenchyme with the plantar epithelium (Fig. 1B), while dorsal skin epithelium was not able to
129 induce appendages in the glabrous plantar mesenchyme (Fig. 1B), indicating that the dorsal
130 mesenchyme is inductive even prior to DC formation.

131 As DC formation is a gradual process and the first loosely organized Sox2+ cells are found below
132 the emerging placodes from E13.5 onward (Biggs et al., 2018; Gupta et al., 2019), small DCs might
133 already exist at E13.5. Therefore, we assessed where the hair follicle inductive potential resides
134 prior to any known molecular or morphological signs of hair follicle formation by recombining
135 tissues from E12.5 embryos. While the homotypic control recombination of the back skin formed
136 appendages and the corresponding recombination of plantar tissues did not (Fig. 1C), we again

observed appendages in the heterotypic recombinants consisting of the dorsal skin mesenchyme and glabrous plantar epithelium, but not in explants of dorsal skin epithelium and plantar mesenchyme (Fig. 1C). Quantification of all E12.5-E14.5 recombinant explants confirmed that only mesenchymal back skin was inductive (Fig 1D). These data imply that the hair-inductive potential resides in the mesenchyme, even prior to DC formation.

To characterise the appendages that formed in the E12.5 tissue recombinants, epithelia were collected from R26R$^{floxedTomato/+}$;K17-GFP; embryos in which tdTomato (tdT) is ubiquitously expressed and the nascent hair placodes are marked by K17-GFP reporter expression (Bianchi et al., 2005) and the mesenchyme from wild type littermates. Homotypic back skin recombinations served as a positive control revealing strong K17-GFP expression in developing hair follicles (Fig. 2A). Likewise, K17-GFP expression marked the appendages formed in recombinants between back skin mesenchyme and plantar epithelium, however, recombinants of the back skin epithelium with the plantar mesenchyme were devoid of K17-GFP+ appendages (Fig. 2A). Immunostaining with the early hair follicle marker Lhx2 (Rhee, Polak & Fuchs, 2006) not expressed in sweat gland placodes (Cao et al., 2021), and the DC-marker Sox2 (Driskell et al., 2009) verified that the formed appendages were hair follicles (Fig. 2A, Fig. S1A,B).

To ascertain that the mesenchyme harbours hair inductive capacity even in the absence of DC formation, we performed tissue recombination experiments using E12.5 back skin mesenchyme isolated from *Fgf20* null embryos that lack primary and secondary hair follicle DCs (Huh et al., 2013). Indeed, like the wild type mesenchyme, the *Fgf20* null mesenchyme induced formation of appendages when recombined with wild type back skin epithelium, or wild type plantar epithelium (Fig. 2B). These appendages, too, were associated with Sox2+ DCs and Lhx2+ epithelial cells (Fig. 2B, Fig. S1C,D) confirming that the hair follicle inductive capacity of the back skin mesenchyme is independent of DC formation.

Lastly, we asked whether the capacity of the naïve dorsal mesenchyme to induce appendages is restricted to epithelia of epidermal origin by assessing whether hair follicles could form in the oral epithelium. To this end, we recombined non-fluorescent E12.5 back skin mesenchyme with the epithelium of R26R$^{floxedTomato/+}$;K17-GFP embryos, isolated from the E12.5 lower jaw diastema, a toothless region of the oral cavity between the incisor and the molar tooth primordia (Fig. S2A). Back skin epithelium from K17-GFP;R26R$^{floxedTomato/+}$ embryos was used as a control. Again, K17-GFP positive hair follicles readily formed in homotypic back skin control recombinants after 5 days of culture (Fig. 3A). Strikingly, hair follicle-like, K17-GFP+ appendages formed also in explants consisting of the dorsal mesenchyme and the oral epithelium (Fig. 3A). Like the control explants,

170 these appendages expressed Lhx2 and Sox2 in the epithelium and the mesenchyme, respectively.
171 Furthermore, the recombinants generated visible hair shafts after 2 weeks of culture (Fig. 3A, Fig.
172 S2B,C) confirming their hair follicle identity.

173 **Mesenchymal cell density is not significantly increased prior to hair follicle induction**

174 Next, we asked how the mesenchymal primary inductive signal is generated in the mesenchyme. As
175 induction of feather placodes is associated with an increase of mesenchymal cell density (Wessells,
176 1965), we hypothesized that perhaps a similar increase of mesenchymal cell density occurs also
177 during hair follicle induction. Given that Wnt/β-catenin signalling activity is essential for
178 mesenchymal cells to gain DC identity (Atit et al., 2006; Gupta et al., 2019), we analysed Wnt-
179 positive cells.

180 To assess mesenchymal cell density, we produced confocal 3D image stacks of transversal
181 vibratome sections from mouse embryos prior to hair follicle induction at E12.5 and at the time of
182 hair induction at E13.5 (Fig. 4A). We quantified the density of mesenchymal nuclei within 80 µm
183 distance from the epithelium and calculated nuclear densities as average rolling densities in 20 µm
184 windows at 1 µm intervals (Fig. S3A). For statistical analysis, the data was binned at 20 µm
185 intervals. Although cell densities were significantly higher closest to the epithelium at both stages
186 analysed, no difference was observed between E12.5 and E13.5 (Fig. 4B).

187 To assess the distribution of Wnt-activated cells, we took advantage of the TCF/Lef1:H2B-GFP
188 Wnt signalling reporter mouse (Ferrer-Vaquer et al., 2010) and calculated the average rolling
189 density of GFP+ dermal cells at both stages (Fig. S3B). Highest density of TCF/Lef1:H2B-GFP
190 positive cells was observed in the proximity of the epithelium, confirmed by statistical analysis of
191 the binned data, yet there was no difference between the two stages (Fig. 4C). These results suggest
192 that the signal initiating the formation of hair follicles likely arises through changes in gene
193 expression of the mesenchymal fibroblasts rather than via an increase in their density or change in
194 the proportion of Wnt/β-catenin activated cells.

195 **Inhibition of BMP signalling affects placode patterning, but is not sufficient to induce hair**
196 **follicle development**

197 We next aimed to gain insights on the molecular composition of the mesenchymally-derived hair
198 follicle inductive signal using a candidate approach. The evidence showing that Bmp signalling
199 inhibits hair placode formation (Botchkarev et al., 1999; Plikus et al., 2004; Mou et al., 2006;
200 Pummila et al., 2007) led us to hypothesize that downregulation of BMP signalling activity could be

201 sufficient to initiate formation of hair follicles. However, in addition to *Noggin*, numerous other
202 Bmp antagonists are expressed in the embryonic skin mesenchyme at the time of hair follicle
203 induction(Sennett et al., 2015; Jacob et al., 2022 preprint, http://kasperlab.org/embryonicskin)
204 making a genetic approach challenging. Therefore, to test our hypothesis, we inhibited BMP
205 signalling with LDN193189, a small molecule inhibitor of BMP type I receptors (Cuny et al.,
206 2008). Back skin of E12.5 Fgf20$^{\beta Gal/+}$ embryos were cultured with 1 μM LDN193189 for 12 and
207 24h and hair placode induction was assessed by analysing the expression of hair placode markers
208 Fgf20 (using anti-β-Gal staining as a surrogate) and Edar by whole-mount immunostaining
209 (WMIF). Unsatisfyingly, suppression of Bmp activity did not induce precocious hair follicle
210 formation at 12 hours (Fig. 5A). However, when placodes started to emerge after 24h culture, they
211 were larger and less regular in size in LDN193189-treated explants compared to controls (Fig. 5B).

212 **Rspo1 signalling alone is insufficient to induce hair follicle induction**

213 Given the essential role of epithelial Wnt/β-cat signalling in hair follicle induction (Zhang et al.,
214 2009; Huelsken et al., 2001; Närhi et al., 2008; Zhang et al., 2008), we next focused our attention to
215 potential activators of this pathway. As dermal deletion of *Wls*, a gene indispensable for Wnt ligand
216 secretion, does not impair hair follicle induction (Chen et al., 2012), we hypothesized that the
217 inductive signal could be another type of soluble Wnt agonist. R-spondins-1-4 (Rspo1-4) act
218 synergistically with Wnt ligands to enhance Wnt/β-catenin signalling activity via Leucine Rich
219 Repeat Containing G Protein-coupled Receptors 4-6 (Lgr4-6) (Nusse & Clevers, 2017; Steinhart &
220 Angers, 2018). Intriguingly, *Lgr4* and *Lgr6* are expressed in the nascent primary hair placodes
221 (Sennett et al., 2015; Tomann et al., 2016; Snippert et al., 2010) and loss of *Lgr4* leads to near total
222 absence of primary hair placodes and greatly reduced total number of hair follicles in newborn mice
223 (Mohri et al., 2008) implying an important role for Rspos in hair follicle induction.

224 Previous RNA-seq profiling of E14.5 back skin has indicated that *Rspo1* and *Rspo3*, but not *Rspo2*
225 and *Rspo4*, are expressed in the mesenchyme (Sennett et al., 2015; Mok et al., 2019; Snippert et al.,
226 2010). We first analysed the expression pattern of *Rspo1* and *Rspo3* in the back skin prior to hair
227 follicle induction (E12.5), during hair follicle induction (E13.5), and at placode stage (E14.5) by
228 RNA *in situ* hybridization. We did not observe focal expression of *Rspo1* at any stage, instead the
229 signal appeared homogenous in the entire mesenchyme (Fig. 6A). Expression of *Rspo3* was
230 unpatterned at E12.5 and E13.5, but at E14.5, a punctate expression in the DCs was evident,
231 confirmed by wholemount *in situ* hybridisation (Fig. S4A), in line with RNA-seq profiling of DCs
232 (Sennett et al., 2015). To quantify the expression levels of *Rspo1* and *Rspo3*, we performed qRT-
233 PCR on E12.5-E14.5 mesenchymes. Interestingly, *Rspo1* expression was significantly upregulated

between E12.5 andE13.5 (Fig. 6B), whereas the expression of *Rspo3* did not significantly alter between the stages (Fig. 6B). These data suggest that Rspo1 might be associated with hair follicle induction.

In adult mice, exogenous recombinant Rspo1 injection leads to precocious activation of hair follicle stem cells during the resting phase of the hair cycle (Li et al., 2016). To examine whether Rspo1 is sufficient to induce hair placode formation in the embryonic skin, we cultured E12.5 back skin explants for 12 hours and 24 hours with 100 ng/ml Rspo1. At 12 hours, hair placodes had not formed in control or Rspo1-treated skins (Fig. 6C), whereas after 24 hours of culture, focal expression of placode markers was evident in both samples, indicative of placode induction (Fig. 6D). A higher Rspo1 concentration (500 ng/ml) did not induce precocious placodes either (Fig. S4B).

We also tested whether simultaneous activation of Wnt/β-catenin signalling via supplementation of Rspo1 and inhibition of BMP signalling together would be sufficient to advance hair placode formation. To this end, we cultured E12.5 back skin for 12 hours in media supplemented with 100 ng/ml Rspo1 and 1 μM LDN193189, or BSA and DMSO as vehicle controls, but observed no formation of hair placodes in either condition (Fig. 6G). When hair placodes emerged after 24 hours of culture, they were more irregular and even stripe-like in samples supplemented with Rspo1 and LDN193189 (Fig. 6F), similar to those treated with LDN193189 alone (Fig. 5B). Taken together, *ex vivo* manipulation of the developing skin with Rspo1 and LDN193189, alone or together, was not sufficient to induce precocious hair placode formation.

These results raised the question whether exogenous Rspo1 can induce a Wnt signalling response in the naïve epidermis, prior to placode formation. To assess this, we treated E12.5 embryonic skin with 100 ng/ml recombinant Rspo1 in hanging drops for 4 hours and measured the signalling response by analysing expression of placode markers and Wnt/β-catenin target genes *Fgf20* and *Dkk4* (Bazzi et al., 2007; Fliniaux et al., 2008; Huh et al., 2013) by qRT-PCR. We observed a significant increase in the expression of both *Dkk4* (53.66-fold ± 29.27) and *Fgf20* (4.90-fold ± 1.61) upon Rspo1 treatment (Fig. 6E) indicative of a positive Wnt signalling response.

Discussion

To date, the source of the hair follicle inductive signal has remained unknown. Here we show that the hair-forming back skin mesenchyme induces hair development in the normally hairless plantar

epithelium at developmental stages after DC formation (E14.5), at the time of epithelial thickening (E13.5), as well as prior to DC formation (E12.5). Even the E12.5 *Fgf20* null mesenchyme that is devoid of primary and secondary hair follicle DCs induced hair follicle formation in the normally glabrous epithelium. These data confirm that the mesenchyme is the source of the inductive cue(s) even prior to any molecular or morphological signs of hair follicle induction. This contrasts with the observations of the developing tooth where the tooth inductive capacity resides initially in the epithelium, but shifts to the mesenchyme concomitant with the condensation of the dental mesenchyme (Mina & Kollar, 1987; Lumsden, 1988). In our recombination experiments, the back skin epithelium failed to induce hair follicle formation at all stages analysed.

In developing chicken embryos, a global increase in mesenchymal cell density precedes feather follicle induction (Wessells, 1965; Ho et al., 2019). We found no evidence for a similar change in the upper dermis of mouse embryos at the time of hair placode formation suggesting that alterations in cellular gene expression levels rather than cell density govern hair follicle induction. The identity of the hair follicle inductive signal remains elusive to date. However, all available evidence points to positive and negative roles for the Wnt/β-catenin and Bmp signalling pathways, respectively (Biggs & Mikkola, 2014). Here, we assessed the ability of the Bmp receptor inhibitor LDN193189 and Wnt agonist Rspo1 to induce hair follicle development. Although suppression of Bmp signalling changed the regular arrangement of the primary hair placodes into a stripe-like pattern, in line with its proposed involvement in hair follicle patterning (Mou et al., 2006; Glover et al., 2017), it did not result in precocious placode formation. *In vivo,* hair follicle formation is suppressed when *Noggin* is ablated (Botchkarev et al., 1999, 2002), while its overexpression leads to formation of excess and ectopic follicles (Plikus et al., 2004). In cultured skin explants, exogenous Bmp4 prevents placode formation (Mou et al., 2006; Pummila et al., 2007). Together these results show that Bmp signalling plays a central role in hair follicle induction and patterning, yet its inhibition alone appears to be insufficient to trigger hair follicle development. In developing skin, downregulation of epithelial Bmp activity might be achieved via concomitant downregulation of pathway agonists (such as Bmp4) and upregulation of soluble antagonists, many of which are expressed in the mesenchyme at the time of hair follicle induction (Jacob et al., 2022 preprint; Sennett et al., 2015).

Augmentation of Wnt signalling via application of Rspo1 alone or together with LDN193189 did not induce precocious hair follicle development either, although we did observe a significant upregulation of hair placode marker genes *Dkk4* and *Fgf20* upon Rspo1 treatment at E12.5, providing evidence that the naïve epidermis is responsive to Rspo1 prior to hair follicle induction.

While the failure in hair placode induction may indicate that additional signalling pathways are necessary, alternative explanations are also plausible. The periodic organization of hair follicles is thought to arise via the Turing reaction-diffusion system (Andl et al., 2002; Sick et al., 2006; Mou et al., 2006; Glover et al., 2017). This self-organizing model posits that spatial patterns result from the interaction of diffusible signals that minimally consist of a pair of interacting diffusible chemical signals: a short-range, self-enhancing activator and an activator-induced, longer-range inhibitor (Turing, 1952; Gierer & Meinhardt, 1972; Kondo, Miura & Turing, 2010). As this system leads to focal production of both the activator and the inhibitor, supplying the activator (such as Rspo1) in the culture medium might initially flatten the Wnt activity pattern and thereby prevent follicle induction. It is also possible that Rspo1 alone is not sufficient to increase Wnt signalling activity above a critical threshold. We speculate that to achieve this threshold, combined upregulation of mesenchymally produced agonists (such as Rspo1) and downregulation of antagonists (such as Dkks and Secreted Frizzled-related proteins, Sfrps) might be necessary. Indeed, a recent transcriptomic profiling study revealed strong downregulation of *Dkk2* in the upper dermis at the time of hair follicle induction (Jacob et al., 2022 preprint). *Dkk2* is also expressed at higher levels in the non-hairy regions of the embryonic skin compared to the hair-forming regions, and its deletion is sufficient to induce ectopic hair follicle formation in the plantar skin (Song et al., 2018) and cornea (Mukhopadhyay et al., 2006), underscoring the significance of diffusible mesenchymal Wnt inhibitors in hair follicle induction.

Taken together, our study complements the tissue recombination studies of inductive signalling in hair follicle development by establishing that the primary inductive cue arises from the mesenchyme. While the identity of the signal remains elusive, our results from back skin mesenchyme-oral epithelium recombination experiments reveal that the hair inductive cue is readily interpreted also by a tissue of non-skin origin resulting in the formation of functional hair follicles. Recombination of DC-containing whisker pad mesenchyme with the dental epithelium has demonstrated that under the inductive signals of the DC, the dental epithelium switches from the tooth-forming program to one generating whiskers (Kollar, 1970, 1966). As the oral epithelium used in our experiments was devoid of tooth placodes, our interpretation is that E12.5 back skin mesenchyme induced hair follicles *de novo*, rather than by transforming an existing tooth primordium into a hair-producing organ. Instead, genetic activation of epithelial Wnt signalling induces ectopic epithelial invaginations and teeth, not hair follicles, in the oral epithelium (Närhi et al., 2008; Zhang et al., 2008; Wang et al., 2009). This together with our results imply that hair follicle identity is governed by mesenchymal cues other than those merely intensifying epithelial

331 Wnt activity and placode formation. Importantly, our results demonstrate that hair follicle inductive
332 capacity is an intrinsic property of the naïve skin mesenchyme even prior to formation of the dermal
333 condensate.

334

335 **Materials and Methods**

336 **Mouse lines**

Mouse line	Source or reference	Identifiers
wildtype NMRI	Laboratory animals centre, Helsinki institute of Life Science, University of Helsinki	
Fgf20$^{\beta\text{-Gal}/\beta\text{-Gal}}$	PMID: 23431057	RRID:MGI:5425887
K17-GFP	PMID: 16055733, Jackson Laboratory	Stock: 023965, RRID:IMSR_JAX:023965
R26R^{tdTomato}	Jackson Laboratory	Stock 007914
Pgk-Cre	PMID: 9608738, Jackson Laboratory	RRID:IMSR_JAX:020811
R26R^{tdTomato}	PMID:20023653, Jackson Laboratory	Stock 007914, RRID:IMSR_JAX:007914
R26R^{mTmG}	Jackson Laboratory	Stock 007576, RRID:IMSR_JAX:007576
TCF/Lef1:H2B-GFP	Jackson Laboratory	Stock 013752, RRID:IMSR_JAX:013752

337

338 **Antibodies**

Antibody	Producer	Identifiers
goat, Sox2	Santa Cruz	SC-17320
rabbit, Sox2	Stemgent	09-0024
goat, Lhx2	Santa Cruz	SC-19344
rat, EpCAM	BD Pharmingen	552370

339

340 **Reagents and kits**

Reagent	Producer	Identifiers
RSPO1, Recombinant Mouse R-spondin1 (CHO-exp) Protein, CF	R&D Systems	cat. 7150-RS-050/CF
Stemolecule™ LDN193189	Stemgent (Lexington, MA)	cat. 04-0074
RNEase Plus Mini Kit	Qiagen, GmbH	REF. 74126
iScript gDNA Clear cDNA Synthesis Kit	Bio-Rad (Hercules, CA)	cat. 1725035
Dkk4, Mmu, FAM Probe Assay	Bio-Rad (Hercules, CA)	cat. 10031225
GAPDH, Mmu, Cy5 Probe Assay	Bio-Rad (Hercules, CA)	cat. 10031231
Fgf20, Mmu, TEX615 Probe Assay	Bio-Rad (Hercules, CA)	cat. 10031234
iTaq Universal Probes Supermix	Bio-Rad (Hercules, CA)	cat. 1725131
Höchst33342	Invitrogen	REF. H3570
Proteinase K	Roche	REF 3115879001

341

342 **Ethics statement**

343 All mouse studies were approved and carried out in accordance with the guidelines of the Finnish
344 national animal experimentation board.

345 **Mouse lines**

346 R26R^{mTmG} mouse line was obtained from Jackson Laboratory and, as previously described in (Lan
347 et al., 2023 preprint), crossed to Pgk-Cre to obtain mice where R26R^{mTmG} is recombined to
348 R26R^{mG}, and constitutively and heritably expressed from the Rosa26 locus in every cell.
349 R26R^{tdTomato} line was obtained from Jackson Laboratory and crossed to Pgk-Cre (also from Jackson
350 Laboratory, Stock: 020811) to obtain mice where tdTomato is constitutively and heritably
351 expressed from the Rosa26 locus in every cell. In hanging drop experiments, wild type NMRI
352 embryos were used.

353 **Tissue recombination**

354 The back skins were dissected from embryos of the indicated stages and genotypes. To obtain the
355 plantar skin, the entire distal part of the limb was dissected. To obtain the diastema tissue from
356 lower jaws, the mandible was dissected and trimmed to contain only the lingual surface of the
357 mandible with the incisor and molar tooth primordia to mark borders of the diastema. The dissected
358 tissues were treated with 2.5 U/ml Dispase II (Roche) in PBS, +4ºC for the following times: E12.5
359 dorsal and plantar skin 20 min, E13.5 back skin 25-30 min, E14.5 40 min, oral tissue 8 min. The
360 tissues were then allowed to rest in culture medium at room temperature for 30 min. The plantar
361 skin was dissected from the rest of the limb, and all epithelial and mesenchymal tissues separated
362 using forceps and needles. Epithelial and mesenchymal tissues were recombined so that the
363 epithelium was placed on top of the mesenhcyme. Tissue separation efficiency was assessed by
364 microscopy. The separation was always efficient, yet it was not possible to avoid the transfer of
365 single mesenchymal cells with the epithelium.

366 **Ex vivo tissue culture**

367 Tissues were cultured in the air-liquid interface in a Trowell-type setup as described earlier (Närhi
368 & Thesleff, 2010) using DMEM, 10% FBS, 1% penicillin-streptomycin (PS), both supplemented
369 with 10 U/ml penicillin, 10 µg/ml streptomycin, except with recombinations including oral tissues
370 when DMEM:F12 (1:1) supplemented with 10% FBS, 1% PS, and 100 ng/ml ascorbic acid was
371 used. Media were exchanged every other day. When indicated, the media were further
372 supplemented with RSPO1 (R&D Systems), LDN193189 (Stemgent, Lexington, MA) at
373 concentrations indicated in the text, and BSA and DMSO used as vehicle. At the end of the culture,
374 tissues were fixed in 4% paraformaldehyde in PBS for immunofluorescence staining 1 h at room
375 temperature, and washed with PBS.

376 **Vibratome sectioning**

377 To make transversal vibratome sections of E12.5 and E13.5 embryos, the embryos were decapitated
378 and fixed in 4% paraformaldehyde in PBS overnight at +4ºC. The embryos were then embedded in
379 2% low-melting point agarose (Thermo Scientific, Vilnius, Lithuania) in PBS, sectioned to 250 –
380 300 µm sections using Microm HM650 V vibratome, and the sections were collected in PBS prior
381 to immunostaining.

382

383

384 **Immunostaining and confocal microscopy**

385 The fixed tissues were washed in PBS and stained with antibodies using standard protocols. In
386 brief, samples were blocked and permeabilized using PBS, 10% normal donkey serum, 0.3%
387 Triton-X, room temperature, 1 h, followed by overnight incubation at +4°C with the primary
388 antibodies diluted in the blocking solution: Sox2 (1:250), LHX2 (1:400), EpCAM (1:500), β-
389 Galactosidade (1:1000), and Edar (1:400). All samples we co-stained with 1:2000 Hoechst33342.
390 The samples were further washed with several changes of PBS over 6 hours at room temperature
391 prior to incubation with AlexaFluor conjugated secondary antibodies diluted 1:400 in PBS
392 overnight at +4°C. The following day, the samples were washed with several changes of PBS over
393 minimum of 4 h at room temperature and mounted on microscopy slides with Anti-Fade
394 Fluorescense Mounting Medium (Abcam).

395 The samples were imaged using Zeiss LSM 700 laser scanning confocal microscope equipped with
396 PMT using Plan-Apochromat 10x/0.45, LD LCI Plan-Apochromat 25x/0.8 Imm Corr, and LCI
397 Plan-Neofluar 63x/1.30 Imm Corr objectives. To analyse dermal cell density, image stacks of the
398 vibratome sections were obtained using the 63x objective at 0.5 µm intervals. To analyse treated
399 skin explants for placode induction images were obtained with a 10x objective at 5-10 µm intervals.

400 **Image analysis**

401 To quantify mesenchymal cell densities, confocal image stacks of vibratome sections were
402 processed and analysed using Imaris 10.0 and R softwares. Firstly, the attenuation of signal in the
403 sample was determined by measuring average Hoechst33342 signal intensities on the top and
404 bottom z-sections of the stack in 5 - 10 measuring points made on the nuclei. The attenuation
405 correction function of Imaris was then used on the channels of the image. The epithelial surface was
406 created manually based on the anti-EpCAM staining and a distance transformation was made to
407 delimit the 80 µm of the mesenchyme to epithelium. The nuclear Hoechst33342 signal within this
408 volume was then used to segment the nuclei using the machine learning Labkit plugin (Arzt et al.,
409 2022) by classifying Hoechst33342 and background pixels. Distance of the cell to epithelium was
410 determined as the intensity of the distance transformation channel at the centre and the
411 TCF/Lef1:H2B-GFP intensity as the mean intensity of the GFP channel of each segmented nucleus.
412 The volumes at each 1 µm distance interval were determined using the auxiliary ImageJ histogram
413 function, by quantifying the number of pixels with respective values of the distance transformation
414 channels within the delimited 80 µm from the epithelium volume. The densities were calculated,
415 and statistical testing was performed using R-studio software.

416 For *ex vivo* cultured samples, the confocal image stacks were visualised as maximal intensity
417 projections and placode induction was determined as patterned upregulation of Fgf20$^{\beta Gal}$ reporter
418 and Edar expression.

419 **Hanging drop culture, RNA extraction, and qRT-PCR**

420 The short-term treatment of tissue samples in the hanging drop culture was performed as previously
421 described (Biggs et al., 2018). Briefly, in two independent experiments E12.5 skins were dissected
422 from NMRI embryos and cut in half along the dorsal midline. The explants were then placed
423 individually in 40 µl droplets of DMEM, 10% FBS, 1% penicillin-streptomycin supplemented with
424 either 100 ng/ml RSPO1 (R&D Systems) or the respective volume of 0.1% BSA in PBS for vehicle
425 control under a culture dish lid that was turned on a culture dish, and maintained for 4 hours at
426 37°C, 5% CO_2. RNA was extracted from the samples using the RNEasy Plus Mini Kit (Qiagen
427 GmbH, Hilden, Germany) according to manufacturer's instructions. cDNA was synthesized from 1
428 µg RNA using iScript gDNA Clear cDNA Synthesis Kit (BIORAD, Hercules, CA), according to
429 manufacturer's instructions and the cDNA was diluted to 5 ng/µl.

430 For analysis of *Rspo1* and *Rspo3* gene expression, the back skin was dissected from wild type
431 NMRI embryos at E12.5 (N=13), E13.5 (N=12), and E14.5 (N=10), treated with Dispase II as
432 described above to separate the mesenchyme from the epithelium. The mesenchyme was collected,
433 and the RNA extracted, and cDNA translated as above.

434 For embryonic skin samples treated with Rspo1, qRT-PCR was performed using gene-specific
435 PrimePCR Probe Assay (Bio-Rad, Hercules, CA) for mouse *Dkk4*, *Fgf20* and *Gapdh* multiplexed in
436 20 µl reactions according to manufacturer's instructions with 25 ng of template. Reactions were
437 performed in triplicate wells with the CFX96 Real-Time System (Bio-Rad, Hercules, CA) with the
438 protocol described earlier (Biggs et al., 2018). The fold changes were calculated with the Δ ΔCT
439 method (Livak, Schmittgen & Methods, 2001), by normalizing to average of reference gene *Gapdh*
440 in all controls. The normal distribution of statistical difference was analysed using paired Student's
441 T-test.

442 Expression of *Rspo1* and *Rspo3* in the embryonic skin mesenchyme was analysed with primer-
443 based RT-qPCR using Fast-SYBR Green Master Mix (Thermo Fisher Scientific, Vilnius, Lithuania)
444 in 20 µl reactions with 15 ng template and 0.5 µM of each primer. *Rspo1* primers were designed
445 using template NM_138683.2: forward AGAGACAGAGGCGGATCAGTG and reverse
446 CAGAATGAAGAGCTTGGGCG, and *Rspo3* using template NM_028351.3: forward
447 GTCAGTATTGTACACTGTGAGGC and reverse CCGTGTTTCAGTCCCCCTTT. *Gapdh*

448 primers were: forward CTCGTCCCGTAGACAAAATGG and reverse
449 AGATGGTGATGGGCTTCCC. Reactions were run in triplicate as above. The relative expression
450 was calculated using the ΔCT method by normalizing to *Gapdh* and analysed with Student's T-test.

451 **In situ hybridization**

452 For whole-mount RNA *in situ* hybridisation, E14.5 wild type NMRI embryos were decapitated and
453 fixed in 4% PFA in PBS overnight at 4°C, and then dehydrated in a series of methanol. The
454 hybridization was performed manually using a protocol described before (Biggs *et al*. 2018).
455 Antisense RNA probes were designed to target *Rspo1* (template NM-138683.2, base pairs 924-
456 1359) and *Rspo3* (NM-028351.3, base pairs 975-1448). The samples were imaged using Zeiss
457 AxioZoom.V16 stereomicroscope with PlanZ 1.0x/C objective and Axiocam 305 color camera.

458 For radioactive *in situ* hybridization on paraffin sections, the E12.5 (N=4), E13.5 (N=5), and E14.5
459 (N=5) embryos were decapitated, fixed in 4% PFA overnight at 4°C, processed into paraffin blocks
460 using standard protocols, and section in 5 µm sagittal sections. The *in situ* hybridization was
461 performed according to standard protocols (Huh et al., 2013). Imaging and image processing was
462 performed as previously described (Biggs et al., 2018).

463

464 **Acknowledgements**

465 We thank Ms. Raija Savolainen, Ms. Riikka Santalahti, and Ms. Merja Mäkinen for excellent
466 technical assistance, Ms. Verdiana Papagno for assistance with *in situ* hybridization, Dr. Qiang Lan
467 for crosses of mice, Dr. Kimmo Tanhuanpää for expert advice on image analysis, and past and
468 present members of the Mikkola, Jukka Jernvall, and Anamaria Balic labs for stimulating
469 discussions. We thank Dr. Leah Biggs for critical reading of the manuscript. Mouse studies were
470 carried out with the support of HiLIFE Laboratory Animal Center Core Facility, University of
471 Helsinki. Confocal microscopy was conducted at the Light Microscopy Unit, Institute of
472 Biotechnology, supported by HiLIFE and Biocenter Finland.

473

474 **Competing interests**

475 The authors declare no competing interests.

476

Funding

This work was supported by the Sigrid Jusélius Foundation (MLM) and the HiLIFE Fellow Program, University of Helsinki (MLM). OJMM acknowledges support from the graduate program in Integrative Life Sciences (University of Helsinki) and Finnish Cultural Foundation. The funders had no role in study design, data collection and analysis, preparation of the manuscript, or decision to publish.

Author Contributions Statement

Otto Mäkelä: Conceptualization, Methodology, Investigation, Formal Analysis, Writing – Original Draft, Writing – Review & Editing, Visualization

Marja Mikkola: Conceptualization, Methodology, Writing – Review & Editing, Supervision, Project administration, Funding acquisition

References

Ahtiainen, L., Lefebvre, S., Lindfors, P.H., Renvoisé, E., Shirokova, V., Vartiainen, M.K., Thesleff, I. & Mikkola, M.L. (2014) Directional Cell Migration, but Not Proliferation, Drives Hair Placode Morphogenesis. *Developmental Cell*. 28 (5), 588–602. doi:https://doi.org/10.1016/j.devcel.2014.02.003.

Andl, T., Reddy, S.T., Gaddapara, T. & Millar, S.E. (2002) WNT signals are required for the initiation of hair follicle development. *Developmental cell*. 2 (5), 643–653. doi:10.1016/S1534-5807(02)00167-3.

Arzt, M., Deschamps, J., Schmied, C., Pietzsch, T., Schmidt, D., Tomancak, P., Haase, R. & Jug, F. (2022) LABKIT: Labeling and Segmentation Toolkit for Big Image Data. *Frontiers in Computer Science*. 4 (February), 1–12. doi:10.3389/fcomp.2022.777728.

Atit, R., Sgaier, S.K., Mohamed, O.A., Taketo, M.M., Dufort, D., Joyner, A.L., Niswander, L. & Conlon, R.A. (2006) β-catenin activation is necessary and sufficient to specify the dorsal dermal fate in the mouse. *Developmental Biology*. 296 (1), 164–176. doi:10.1016/J.YDBIO.2006.04.449.

504 Bazzi, H., Fantauzzo, K.A., Richardson, G.D., Jahoda, C.A.B. & Christiano, A.M. (2007) The Wnt
505 inhibitor, Dickkopf 4, is induced by canonical Wnt signaling during ectodermal appendage
506 morphogenesis. *Developmental Biology*. 305 (2), 498–507. doi:10.1016/j.ydbio.2007.02.035.

507 Bianchi, N., Depianto, D., McGowan, K., Gu, C. & Coulombe, P.A. (2005) Exploiting the keratin
508 17 gene promoter to visualize live cells in epithelial appendages of mice. *Molecular and cellular*
509 *biology*. 25 (16), 7249–7259. doi:10.1128/MCB.25.16.7249-7259.2005.

510 Biggs, L.C., Mäkelä, O.J., Myllymäki, S.-M., Das Roy, R., Närhi, K., Pispa, J., Mustonen, T. &
511 Mikkola, M.L. (2018) Hair follicle dermal condensation forms via Fgf20 primed cell cycle exit, cell
512 motility, and aggregation. *eLife*. 7. doi:10.7554/eLife.36468.

513 Biggs, L.C. & Mikkola, M.L. (2014) Early inductive events in ectodermal appendage
514 morphogenesis. *Semin Cell Dev Biol*. 25–26, 11–21. doi:10.1016/j.semcdb.2014.01.007.

515 Botchkarev, V.A., Botchkareva, N. V., Roth, W., Nakamura, M., Chen, L.H., Herzog, W., Lindner,
516 G., McMahon, J.A., Peters, C., Lauster, R., McMahon, A.P. & Paus, R. (1999) Noggin is a
517 mesenchymally derived stimulator of hair-follicle induction. *Nature Cell Biology*. 1 (3), 158–164.
518 doi:10.1038/11078.

519 Botchkarev, V.A., Botchkareva, N. V., Sharov, A.A., Gilchrest, B.A., Funa, K. & Huber, O. (2002)
520 Modulation of BMP signaling by noggin is required for induction of the secondary (Nontylotrich)
521 hair follicles. *Journal of Investigative Dermatology*. 118 (1), 3–10. doi:10.1046/j.1523-
522 1747.2002.01645.x.

523 Chen, D., Jarrell, A., Guo, C., Lang, R. & Atit, R. (2012) Dermal β-catenin activity in response to
524 epidermal Wnt ligands is required for fibroblast proliferation and hair follicle initiation.
525 *Development*. 139 (8), 1522–1533. doi:10.1242/dev.076463.

526 Cohen, J. (1961) The Transplantation of Individual Rat and Guinea-pig Whisker Papillae. *Journal*
527 *of Embryology and Experimental Morphology*. 9 (1), 117–127. doi:10.1242/DEV.9.1.117.

528 Cuny, G.D., Yu, P.B., Laha, J.K., Xing, X., Liu, J.F., Lai, C.S., Deng, D.Y., Sachidanandan, C.,
529 Bloch, K.D. & Peterson, R.T. (2008) Structure–activity relationship study of bone morphogenetic
530 protein (BMP) signaling inhibitors. *Bioorganic & Medicinal Chemistry Letters*. 18 (15), 4388–
531 4392. doi:10.1016/J.BMCL.2008.06.052.

532 Dhouailly, D. (1973) Dermo epidermal interactions between birds and mammals: differentiation of
533 cutaneous appendages. *Journal of Embryology and Experimental Morphology*. 30 (3), 587–603.
534 doi:10.1242/dev.30.3.587.

535 Driskell, R.R., Giangreco, A., Jensen, K.B., Mulder, K.W. & Watt, F.M. (2009) Sox2-positive
536 dermal papilla cells specify hair follicle type in mammalian epidermis. *Development*. 136 (16),
537 2815–2823. doi:10.1242/dev.038620.

538 Duverger, O. & Morasso, M.I. (2009) Epidermal patterning and induction of different hair types
539 during mouse embryonic development. *Birth Defects Research Part C: Embryo Today: Reviews*. 87
540 (3), 263–272. doi:10.1002/BDRC.20158.

541 Ferraris, C., Chevalier, G., Favier, B., Jahoda, C.A.B. & Dhouailly, D. (2000) *Adult corneal*
542 *epithelium basal cells possess the capacity to activate epidermal , pilosebaceous and sweat gland*
543 *genetic programs in response to embryonic dermal stimuli*. 5495, 5487–5495.

544 Ferrer-Vaquer, A., Piliszek, A., Tian, G., Aho, R.J., Dufort, D. & Hadjantonakis, A. (2010) A
545 sensitive and bright single-cell resolution live imaging reporter of Wnt/ß-catenin signaling in the
546 mouse. *BMC Developmental Biology*. 10 (1), 121.

547 Fliniaux, I., Mikkola, M.L., Lefebvre, S. & Thesleff, I. (2008) Identification of dkk4 as a target of
548 Eda-A1/Edar pathway reveals an unexpected role of ectodysplasin as inhibitor of Wnt signalling in
549 ectodermal placodes. *Dev Biol*. 320 (1), 60–71. doi:10.1016/j.ydbio.2008.04.023.

550 Gierer, A. & Meinhardt, H. (1972) Gierer-1972-THEORY OF BIOLOGICAL.pdf. *Kybernetik*. 39,
551 30–39. https://link.springer.com/content/pdf/10.1007%2FBF00289234.pdf.

552 Glover, J.D., Wells, K.L., Matthaus, F., Painter, K.J., Ho, W., Riddell, J., Johansson, J.A., Ford,
553 M.J., Jahoda, C.A.B., Klika, V., Mort, R.L. & Headon, D.J. (2017) Hierarchical patterning modes
554 orchestrate hair follicle morphogenesis. *PLoS Biol*. 15 (7), e2002117.
555 doi:10.1371/journal.pbio.2002117.

556 Gupta, K., Levinsohn, J., Linderman, G., Chen, D., Sun, T.Y., Dong, D., Taketo, M.M., Bosenberg,
557 M., Kluger, Y., Choate, K. & Myung, P. (2019) Single-Cell Analysis Reveals a Hair Follicle
558 Dermal Niche Molecular Differentiation Trajectory that Begins Prior to Morphogenesis.
559 *Developmental Cell*. 48 (1), 17-31.e6. doi:10.1016/J.DEVCEL.2018.11.032.

560 Hardy, M.H. (1992) The secret life of the hair follicle. *Trends Genet*. 8 (2), 55–61.
561 https://www.ncbi.nlm.nih.gov/pubmed/1566372.

562 Higgins, C.A., Chen, J.C., Cerise, J.E., Jahoda, C.A. & Christiano, A.M. (2013)
563 Microenvironmental reprogramming by three-dimensional culture enables dermal papilla cells to
564 induce de novo human hair-follicle growth. *Proc Natl Acad Sci U S A*. 110 (49), 19679–19688.
565 doi:10.1073/pnas.1309970110.

566 Ho, W.K.W., Freem, L., Zhao, D., Painter, K.J., Woolley, T.E., et al. (2019) *Feather arrays are*
567 *patterned by interacting signalling and cell density waves*. doi:10.1371/journal.pbio.3000132.

568 Huelsken, J., Vogel, R., Erdmann, B., Cotsarelis, G. & Birchmeier, W. (2001) β-Catenin controls
569 hair follicle morphogenesis and stem cell differentiation in the skin. *Cell*. 105 (4), 533–545.
570 doi:10.1016/S0092-8674(01)00336-1.

571 Huh, S.-H., Närhi, K., Lindfors, P.H., Häärä, O., Yang, L., Ornitz, D.M. & Mikkola, M.L. (2013)
572 Fgf20 governs formation of primary and secondary dermal condensations in developing hair
573 follicles. *Genes & Development*. 27 (4), 450–458. doi:10.1101/gad.198945.112.

574 Jacob, T., Annusver, K., Czarnewski, P., Dalessandri, T., Kastriti, M.E., Levron, C.L., Mikkola,
575 M.L., Rendl, M., Lichtenberger, B.M., Donati, G., Björklund, Å. & Kasper, M. (2022) Molecular
576 and spatial design of early skin development. *bioRxiv*. 2022.12.28.522081.
577 doi:10.1101/2022.12.28.522081.

578 Jahoda, C.A.B., Horne, K.A., Mauger, A., Bard, S. & Sengel, P. (1992) Cellular and extracellular
579 involvement in the regeneration of the rat lower vibrissa follicle. *Development (Cambridge,*
580 *England)*. 114 (4), 887–897. doi:10.1242/DEV.114.4.887.

581 Jamora, C., DasGupta, R., Kocieniewski, P. & Fuchs, E. (2003) Links between signal transduction,
582 transcription and adhesion in epithelial bud development. *Nature*. 422 (6929), 317–322.
583 doi:10.1038/NATURE01458.

584 Kollar, E.J. (1966) An in vitro study of hair and vibrissae development in embryonic mouse skin.
585 *The Journal of investigative dermatology*. 46 (3), 254–262. doi:10.1038/jid.1966.40.

586 Kollar, E.J. (1970) The Induction of Hair Follicles by Embryonic Dermal Papillae. *Journal of*
587 *Investigative Dermatology*. 374–378.

588 Kollar, E.J. & Baird, G.R. (1970) Tissue interactions in embryonic mouse tooth germs. II. The
589 inductive role of the dental papilla. *Journal of embryology and experimental morphology*. 24 (1),
590 173–186. https://pubmed.ncbi.nlm.nih.gov/5487155/.

591 Kondo, S., Miura, T. & Turing, T. (2010) Reaction-Diffusion Model as a. *Science (New York, N.Y.)*.
592 329 (September), 1616–1620.

593 Lan, Q., Trela, E., Lindström, R., Satta, J., Christensen, M.M., Holzenberger, M., Jernvall, J. &
594 Mikkola, M.L. (2023) On growth and form of the mammary gland: Epithelial-mesenchymal
595 interactions in embryonic mammary gland development. *bioRxiv*. 2023.04.24.538064.
596 doi:10.1101/2023.04.24.538064.

597 Li, K.N. & Tumbar, T. (2021) Hair follicle stem cells as a skin-organizing signaling center during
598 adult homeostasis. *The EMBO Journal*. 40 (11). doi:10.15252/EMBJ.2020107135.

599 Li, N., Liu, S., Zhang, H.S., Deng, Z.L., Zhao, H.S., Zhao, Q., Lei, X.H., Ning, L.N., Cao, Y.J.,
600 Wang, H. Bin, Liu, S. & Duan, E.K. (2016) Exogenous R-Spondin1 Induces Precocious Telogen-
601 to-Anagen Transition in Mouse Hair Follicles. *International Journal of Molecular Sciences*. 17 (4).
602 doi:10.3390/IJMS17040582.

603 Livak, K.J., Schmittgen, T.D. & Methods (2001) Analysis of relative gene expression data using
604 real-time quantitative PCR and the 2(-Delta Delta C(T)) Method. *Methods.* 2001 (4), 402–408.

605 Mina, M. & Kollar, E.J. (1987) The induction of odontogenesis in non-dental mesenchyme
606 combined with early murine mandibular arch epithelium. *Archives of oral biology*. 32 (2), 123–
607 127. doi:10.1016/0003-9969(87)90055-0.

608 Mohri, Y., Kato, S., Umezawa, A., Okuyama, R. & Nishimori, K. (2008) Impaired hair placode
609 formation with reduced expression of hair follicle-related genes in mice lacking Lgr4.
610 *Developmental Dynamics*. 237 (8), 2235–2242. doi:https://doi.org/10.1002/dvdy.21639.

611 Mok, K.W., Saxena, N., Heitman, N., Grisanti, L., Srivastava, D., Muraro, M.J., Jacob, T., Sennett,
612 R., Wang, Z., Su, Y., Yang, L.M., Ma'ayan, A., Ornitz, D.M., Kasper, M. & Rendl, M. (2019)
613 Dermal Condensate Niche Fate Specification Occurs Prior to Formation and Is Placode Progenitor
614 Dependent. *Developmental Cell*. 48 (1), 32-48.e5. doi:10.1016/J.DEVCEL.2018.11.034.

615 Morgan, B.A. (2014) The dermal papilla: An instructive niche for epithelial stem and progenitor
616 cells in development and regeneration of the hair follicle. *Cold Spring Harbor Perspectives in*
617 *Medicine*. 4 (7). doi:10.1101/cshperspect.a015180.

618 Mou, C., Jackson, B., Schneider, P., Overbeek, P.A. & Headon, D.J. (2006) Generation of the
619 primary hair follicle pattern. *Proceedings of the National Academy of Sciences of the United States*
620 *of America*. 103 (24), 9075–9080. doi:10.1073/PNAS.0600825103.

621 Mukhopadhyay, M., Gorivodsky, M., Shtrom, S., Grinberg, A., Niehrs, C., Morasso, M.I. &
622 Westphal, H. (2006) Dkk2 plays an essential role in the corneal fate of the ocular surface
623 epithelium. *Development*. 133 (13), 2595. doi:10.1242/dev.02462.

624 Närhi, K., Jarvinen, E., Birchmeier, W., Taketo, M.M., Mikkola, M.L. & Thesleff, I. (2008)
625 Sustained epithelial beta-catenin activity induces precocious hair development but disrupts hair
626 follicle down-growth and hair shaft formation. *Development*. 135 (6), 1019–1028.
627 doi:10.1242/dev.016550.

628 Närhi, K. & Thesleff, I. (2010) Explant culture of embryonic craniofacial tissues: analyzing effects
629 of signaling molecules on gene expression. *Methods Mol Biol*. 666, 253–267. doi:10.1007/978-1-
630 60761-820-1_16.

631 Nusse, R. & Clevers, H. (2017) Wnt/β-Catenin Signaling, Disease, and Emerging Therapeutic
632 Modalities. *Cell*. 169 (6), 985–999. doi:10.1016/J.CELL.2017.05.016.

633 Oliver, R.F. (1970) The induction of hair follicle formation in the adult hooded rat by vibrissa
634 dermal papillae. *J Embryol Exp Morphol*. 23 (1), 219–236.
635 https://www.ncbi.nlm.nih.gov/pubmed/4926619.

636 Plikus, M., Wang, W.P., Liu, J., Wang, X., Jiang, T.X. & Chuong, C.M. (2004) Morpho-Regulation
637 of Ectodermal Organs: Integument Pathology and Phenotypic Variations in K14-Noggin
638 Engineered Mice through Modulation of Bone Morphogenic Protein Pathway. *The American*
639 *Journal of Pathology*. 164 (3), 1099–1114. doi:10.1016/S0002-9440(10)63197-5.

640 Pummila, M., Fliniaux, I., Jaatinen, R., James, M.J., Laurikkala, J., Schneider, P., Thesleff, I. &
641 Mikkola, M.L. (2007) Ectodysplasin has a dual role in ectodermal organogenesis: inhibition of Bmp
642 activity and induction of Shh expression. *Development*. 134 (1), 117–125. doi:10.1242/DEV.02708.

643 Rhee, H., Polak, L. & Fuchs, E. (2006) Lhx2 maintains stem cell character in hair follicles. *Science*.
644 312 (5782), 1946–1949. doi:10.1126/science.1128004.

645 Schmidt-Ullrich, R., Tobin, D.J., Lenhard, D., Schneider, P., Paus, R. & Scheidereit, C. (2006) NF-
646 kappaB transmits Eda A1/EdaR signalling to activate Shh and cyclin D1 expression, and controls
647 post-initiation hair placode down growth. *Development (Cambridge, England)*. 133 (6), 1045–1057.
648 doi:10.1242/DEV.02278.

649 Sennett, R. & Rendl, M. (2012) Mesenchymal–epithelial interactions during hair follicle
650 morphogenesis and cycling. *Seminars in Cell & Developmental Biology*. 23 (8), 917–927.
651 doi:10.1016/J.SEMCDB.2012.08.011.

652 Sennett, R., Wang, Z., Rezza, A., Grisanti, L., Roitershtein, N., Sicchio, C., Mok, K.W., Heitman,
653 N.J., Clavel, C., Ma'ayan, A. & Rendl, M. (2015) An Integrated Transcriptome Atlas of Embryonic
654 Hair Follicle Progenitors, Their Niche, and the Developing Skin. *Dev Cell*. 34 (5), 577–591.
655 doi:10.1016/j.devcel.2015.06.023.

656 Sick, S., Reinker, S., Timmer, J. & Schlake, T. (2006) *WNT and DKK Determine Hair Follicle*
657 *Spacing Through a Reaction-Diffusion Mechanism*. 314 (December), 1447–1451.

658 Snippert, H.J., Haegebarth, A., Kasper, M., Jaks, V., van Es, J.H., Barker, N., van de Wetering, M.,
659 van den Born, M., Begthel, H., Vries, R.G., Stange, D.E., Toftgård, R. & Clevers, H. (2010) Lgr6
660 Marks Stem Cells in the Hair Follicle That Generate All Cell Lineages of the Skin. *Science*. 327
661 (5971), 1385–1389. doi:10.1126/science.1184733.

662 Song, Y., Boncompagni, A.C., Kim, S.S., Gochnauer, H.R., Zhang, Y., Loots, G.G., Wu, D., Li, Y.,
663 Xu, M. & Millar, S.E. (2018) Regional Control of Hairless versus Hair-Bearing Skin by Dkk2. *Cell*
664 *Reports*. 25 (11), 2981-2991.e3. doi:10.1016/j.celrep.2018.11.017.

665 Steinhart, Z. & Angers, S. (2018) Wnt signaling in development and tissue homeostasis.
666 *Development (Cambridge, England)*. 145 (11). doi:10.1242/DEV.146589.

667 Thesleff, I., Vaahtokari, A. & Partanen, A.M. (1995) Regulation of organogenesis. Common
668 molecular mechanisms regulating the development of teeth and other organs. *International Journal*
669 *of Developmental Biology*. 39 (1), 35–50.

670 Tomann, P., Paus, R., Millar, S.E., Scheidereit, C. & Schmidt-Ullrich, R. (2016) Lhx2 is a direct
671 NF-κB target gene that promotes primary hair follicle placode down-growth. *Development*
672 *(Cambridge)*. 143 (9), 1512–1522. doi:10.1242/dev.130898.

673 Turing, A. (1952) The Chemical Basis of Morphogenesis. *Philos. Trans. R. Soc. Lond. Ser. B Biol.*
674 *Sci.* 237, 37–72.

675 Wang, X.P., O'Connell, D.J., Lund, J.J., Saadi, I., Kuraguchi, M., Turbe-Doan, A., Cavallesco, R.,
676 Kim, H., Park, P.J., Harada, H., Kucherlapati, R. & Maas, R.L. (2009) Apc inhibition of Wnt
677 signaling regulates supernumerary tooth formation during embryogenesis and throughout
678 adulthood. *Development (Cambridge, England)*. 136 (11), 1939–1949. doi:10.1242/DEV.033803.

Wessells, N.K. (1965) Morphology and Proliferation During Early Feather Development. *Developmental Biology*. 12, 131–153.

Woo, W.M., Zhen, H.H. & Oro, A.E. (2012) Shh maintains dermal papilla identity and hair morphogenesis via a Noggin–Shh regulatory loop. *Genes & Development*. 26 (11), 1235–1246. doi:10.1101/GAD.187401.112.

Zhang, Y., Andl, T., Yang, S.H., Teta, M., Liu, F., Seykora, J.T., Tobias, J.W., Piccolo, S., Schmidt-Ullrich, R., Nagy, A., Taketo, M.M., Dlugosz, A.A. & Millar, S.E. (2008) Activation of beta-catenin signaling programs embryonic epidermis to hair follicle fate. *Development*. 135 (12), 2161–2172. doi:10.1242/dev.017459.

Zhang, Y., Tomann, P., Andl, T., Gallant, N.M., Huelsken, J., Jerchow, B., Birchmeier, W., Paus, R., Piccolo, S., Mikkola, M.L., Morrisey, E.E., Overbeek, P.A., Scheidereit, C., Millar, S.E. & Schmidt-Ullrich, R. (2009) Reciprocal Requirements for EDA/EDAR/NF-κB and Wnt/β-Catenin Signaling Pathways in Hair Follicle Induction. *Developmental Cell*. 17 (1), 49–61. doi:10.1016/j.devcel.2009.05.011.

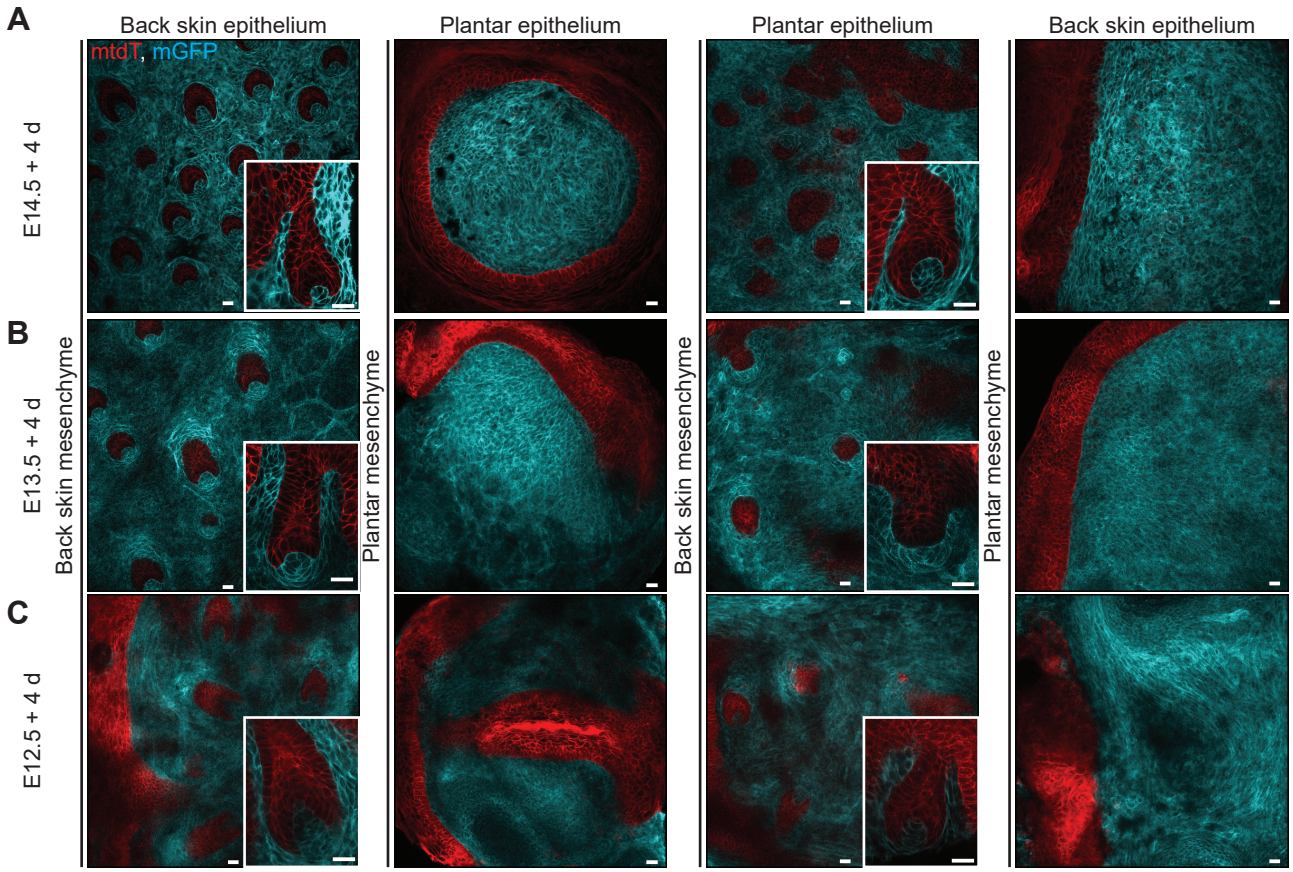

D

	Dorsal epithelium			Plantar epithelium		
Stage	E12.5	E13.5	E14.5	E12.5	E13.5	E14.5
Dorsal mesenchyme	26/31 (83.9%)	14/15 (93.3%)	15/15 (100 %)	27/33 (81.8%)	15/17 (88.2%)	16/19 (84.2%)
Plantar mesenchyme	0/27 (0%)	0/12 (0%)	0/21 (0%)	0/29 (0%)	0/10 (0%)	0/11 (0%)

Fig. 1. Back skin mesenchyme harbors skin appendage inductive capacity even prior to dermal condensate formation. Confocal microscopy optical sections of tissue recombinants consisting of R26R$^{mG/+}$ (cyan) mesenchyme and R26R$^{mTmG/+}$ (red) epithelium from embryonic back skin and plantar skin from E14.5 (A), E13.5 (B), and E12.5 (C) embryos after 4 days of *ex vivo* culture. Insets show individual appendages. Scale = 20 µm. (D) Total number of tissue recombinants of the indicated stages. Numbers indicate recombinants with appendages / total number of recombinants.

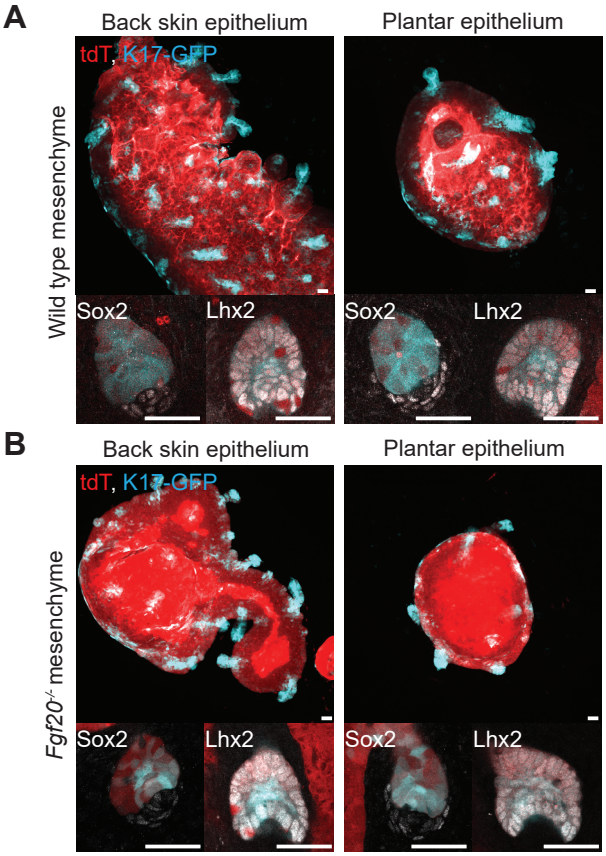

Fig. 2. Wild type and *Fgf20* null back skin mesenchyme-induced skin appendages express hair follicle markers. (A) Maximum intensity projections of confocal microscopy images of tissue recombinants of E12.5 wild type mesenchyme and E12.5 R26R^{floxedTOM};K17-GFP epithelium from back skin (N=11/12) and plantar skin (N=11/12) (left) and optical sections of the same recombinants stained with Sox2 and Lhx2 (right). N indicates recombinants with HFs / total number of recombinants (B) Maximum intensity projections of confocal microscopy images of tissue recombinants of E12.5 Fgf20$^{-/-}$ mesenchyme and E12.5 R26R^{floxedTOM};K17-GFP epithelium from back skin (N=15/17) and plantar skin (N=14/16) (left) and optical sections of the same recombinant stained with Sox2 and Lhx2(right). N indicates recombinants with HFs / total number of recombinants. Scale = 20 µm.

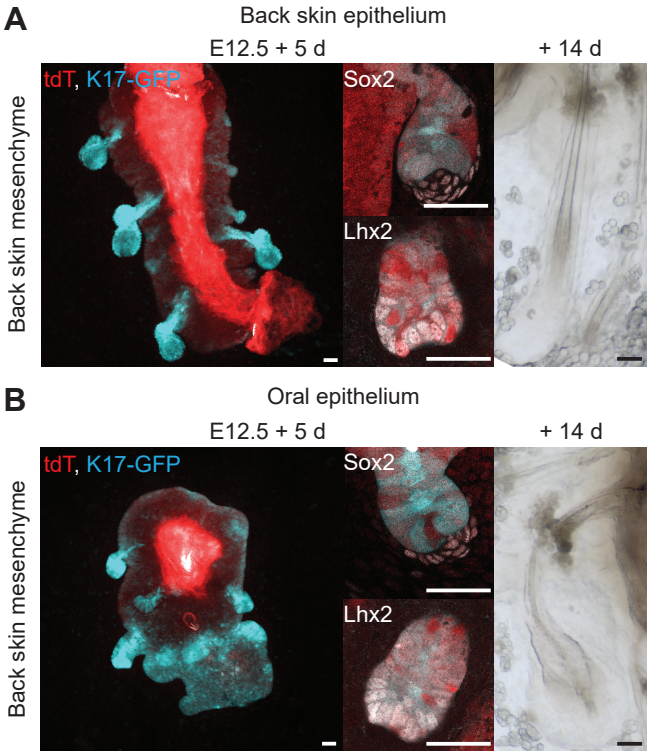

Fig. 3. Naïve back skin mesenchyme induces hair follicles in oral epithelium. Maximum intensity projections of confocal microscopy images (left) of tissue recombinants of E12.5 wild type mesenchyme and (A) E12.5 R26R^{floxedTOM};K17-GFP back skin epithelium (N=10/12), or (B) epithelium from the toothless oral diastema region (N=13/17) after 5 days of *ex vivo* culture. N indicates recombinants with HFs / total recombinants. Optical sections of recombinants stained with Sox2 and Lhx2 (middle), and stereomicrosope images of recombinants cultured for 14 days *ex vivo* (N=5 explants) showing hair follicles producing a hair shaft (right). Scale = 20 µm.

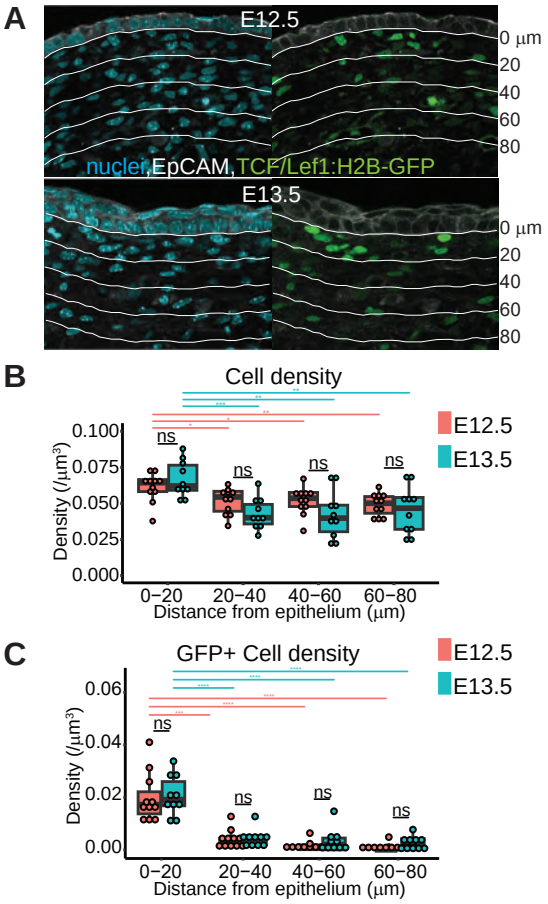

Fig. 4. Mesenchymal cell density is unchanged during hair follicle induction. (A) Confocal optical images of transversal thoracic vibratome sections of E12.5 and E13.5 TCF/Lef1:H2B-GFP embryos stained with Hoechst33342 for nuclei and epithelial marker EpCAM. Lines indicate 20 µm distance intervals from the epithelial-mesenchymal border. Scale = 20 µm. (B) Binned cell densities in 20 µm bins (Mean ±SD) at E12.5 (red) and E13.5 (blue). (C) TCF/Lef1:H2B-GFP+ cell densities at 20 µm bins (Mean ±SD) from the epithelial-mesenhcymal border at E12.5 (red) and E13.5 (blue). $N_{E12.5}$=11 embryos and $N_{E13.5}$=10 embryos. Statistical significance was assessed with Student's T-test.* P<0.05, **P<0.01, ***P<0.001.

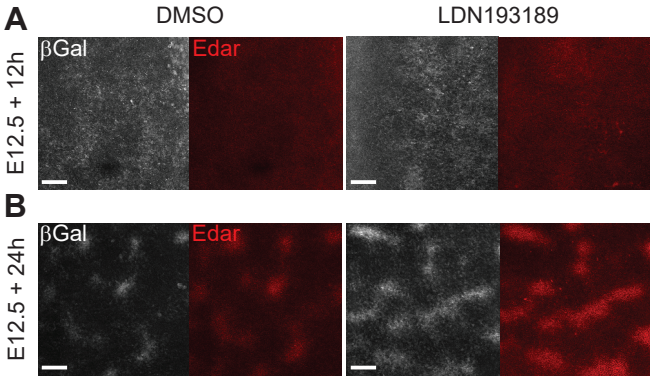

Fig. 5. Inhibition of BMP signalling is insufficient to induce precocious hair placodes. (A, B) Maximum intensity projections of confocal image stacks of DMSO control and LDN193189 (1 μM) treated E12.5 Fgf20$^{\beta Gal/+}$ back skin explants after 12 hours (N = 0/10 for both) and 24 hours (N= 9/11 for both) of culture. Samples were stained with βGal and Edar antibodies to visualize nascent placodes. N indicates samples with induced placodes / total number of samples. Scale = 100 μm.

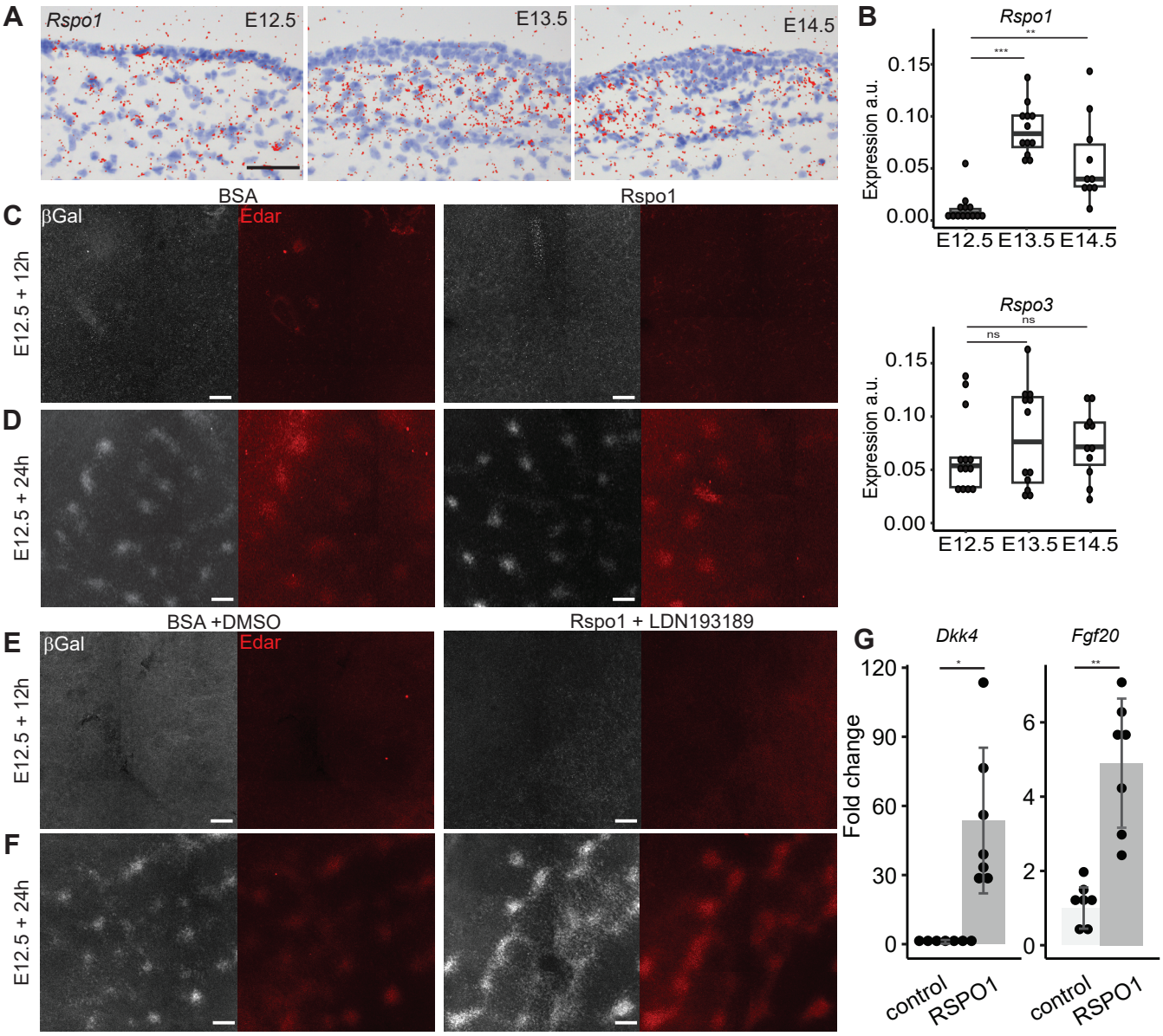

Fig. 6. *Rspo1* is upregulated in dorsal mesenchyme upon hair follicle induction but is not sufficient to induce hair follicle development. (A) *Rspo1* expression in back skin of E12.5, E13.5, and E14.5 wild type embryos, detected by RNA *in situ* hybridization. Scale = 50 µm. (B) qRT-PCR quantification of *Rspo1* and *Rspo3* expression in back skin mesenchyme at E12.5, E13.5, and E14.5 normalized to *Gapdh* expression (Line indicates mean, whiskers variance). * P<0.05, **P<0.01, ***P<0.001, statistical significance was assessed with Student's T-test. (C, D) Maximum intensity projections of confocal image stacks of BSA and Rspo1 (100 ng/ml) treated Fgf20$^{\beta Gal/+}$ E12.5 back skin explants after 12 hours (N = 0/9 for both) and 24 hours (N_{DMSO} = 13/14 and N_{LDN} = 14/15) of culture with βGal and Edar immunolabelling. Numbers indicate samples with induced placodes / total number of samples. Scale = 100 µm. (F, G) Maximum intensity projections of confocal image stacks of BSA + DMSO and Rspo1 (100 ng/ml) + LDN193189 (1µM) treated Fgf20$^{\beta Gal/+}$ E12.5 back skin explants after 12 hours (N = 0/7 for both) and 24 hours (N = 7/7 for both) of culture with βGal and Edar immunolabelling. (E) Fold change of expression of *Dkk4* (53.66 ± 29.27), and *Fgf20* (4.90 ± 1.61) in E12.5 back skin after 4 hours of 100 ng/ml Rspo1 treatment relative to vehicle control, measured by qRT-PCR (N=7, Mean ±SD). *P<0.05, **P<0.01. Statistical significance was assessed with Student's T-test and Wilcoxon matched-pairs signed rank test for normally (*Fgf20*) and non-normally (*Dkk4*) distributed data, respectively.

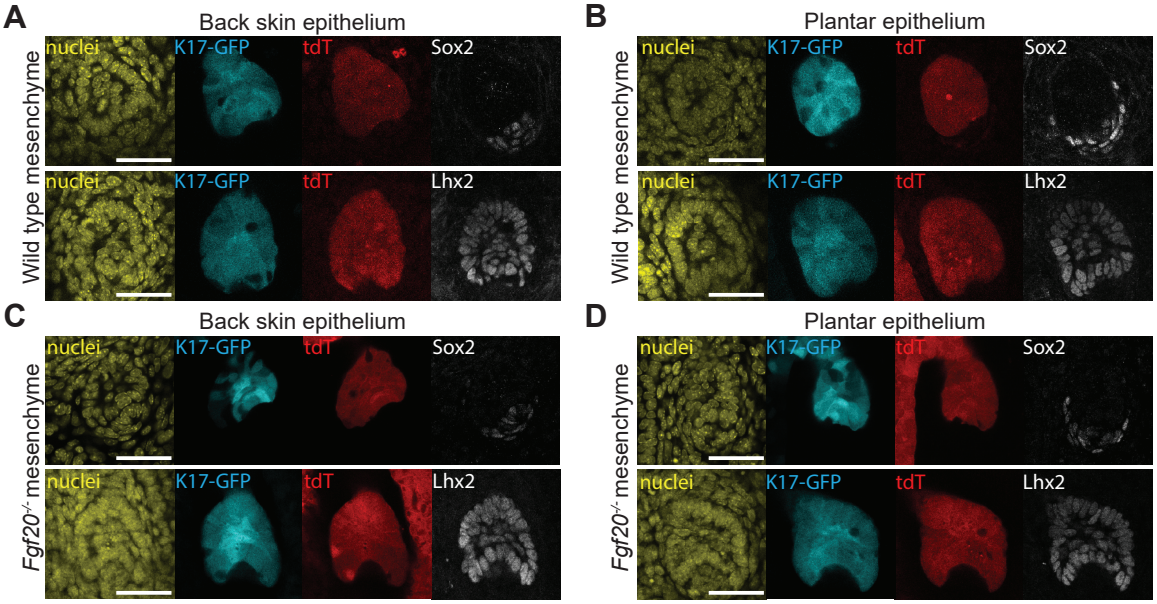

Fig S1 (Related to Fig. 2). **Appendages induced in recombinants of E12.5 wild type or Fgf20$^{-/-}$ back skin mesenchyme and E12.5 plantar epithelium express hair follicle markers.** (A, B) Single channels of the confocal optical sections of recombinants of E12.5 wild type mesenchyme and back skin control (A) and plantar epithelium (B) from E12.5 R26R^{floxedTOM};K17-GFP embryos stained with Sox2 or Lhx2. (C, D) Single channels of the confocal optical sections of recombinants of E12.5 Fgf20$^{-/-}$ mesenchyme and back skin (C) and plantar epithelium (D) from E12.5 R26R^{floxedTOM};K17-GFP embryos stained with Sox2 or Lhx2. Nuclei were stained with Hoecsht33342. Scale 20 µm.

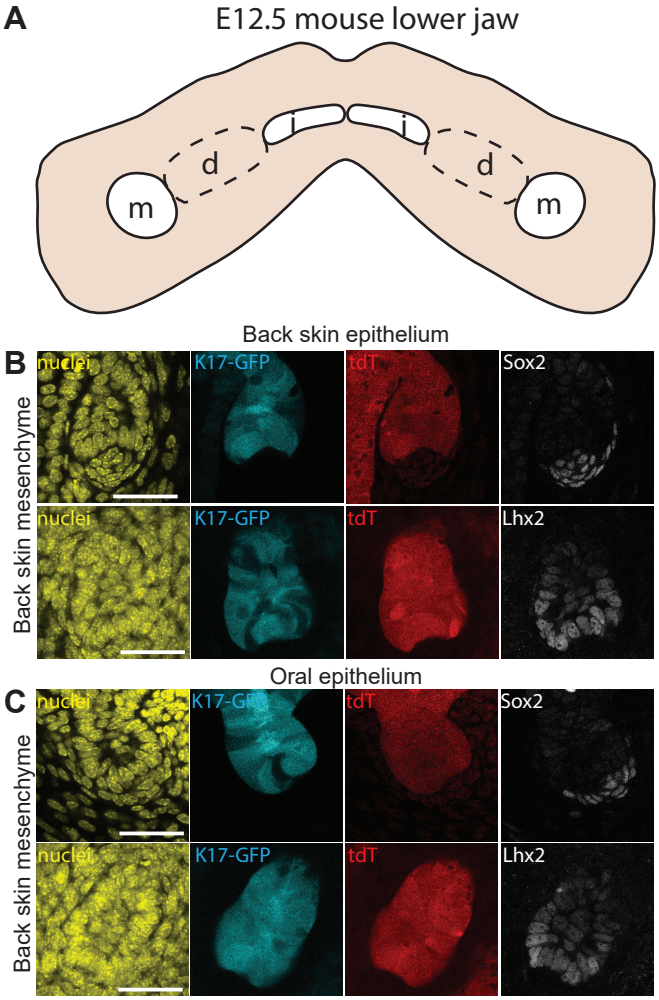

Fig S2 (Related to Fig. 3)**. Appendages induced in recombinants between E12.5 back skin mesenchyme and oral epithelium express hair follicle markers.** (A) A schematic view of the E12.5 mouse lower jaw. White areas indicate incisor (i) and molar (m) primordia and area marked by the dashed line indicates diastema (d) region used in the tissue recombination experiments. (B, C) Single channels of the confocal optical sections from the appendages of the homotypic (B) and heterotypic (C) recombinations in Fig 3. Scale 20 µm.

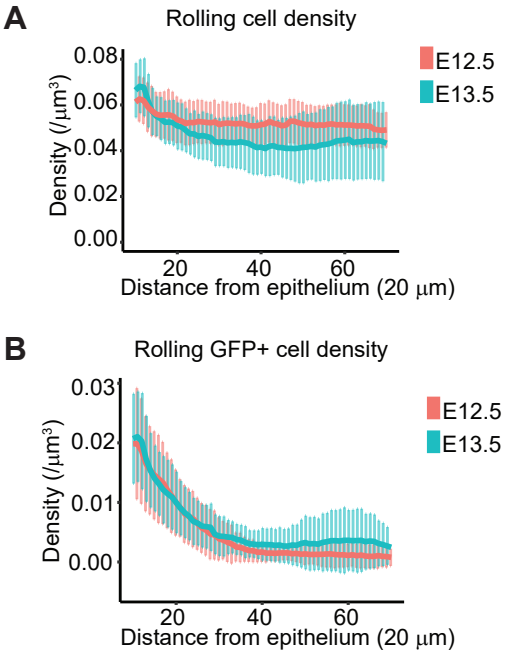

Fig S3 (Related to Fig. 4)**. Mesenchymal cell density does not change during hair follicle induction.** (A) Mean rolling densities of all mesenchymal cells within 20 μm windows at 1 μm intervals (nuclei/μm^3, Mean ±SD) at E12.5 (red) and E13.5 (blue). (B) Mean rolling densities of TCF/Lef1:H2B-eGFP+ cells within 20 μm windows at 1 μm intervals (nuclei/μm^3, Mean ±SD) at E12.5 (red) and E13.5 (blue).

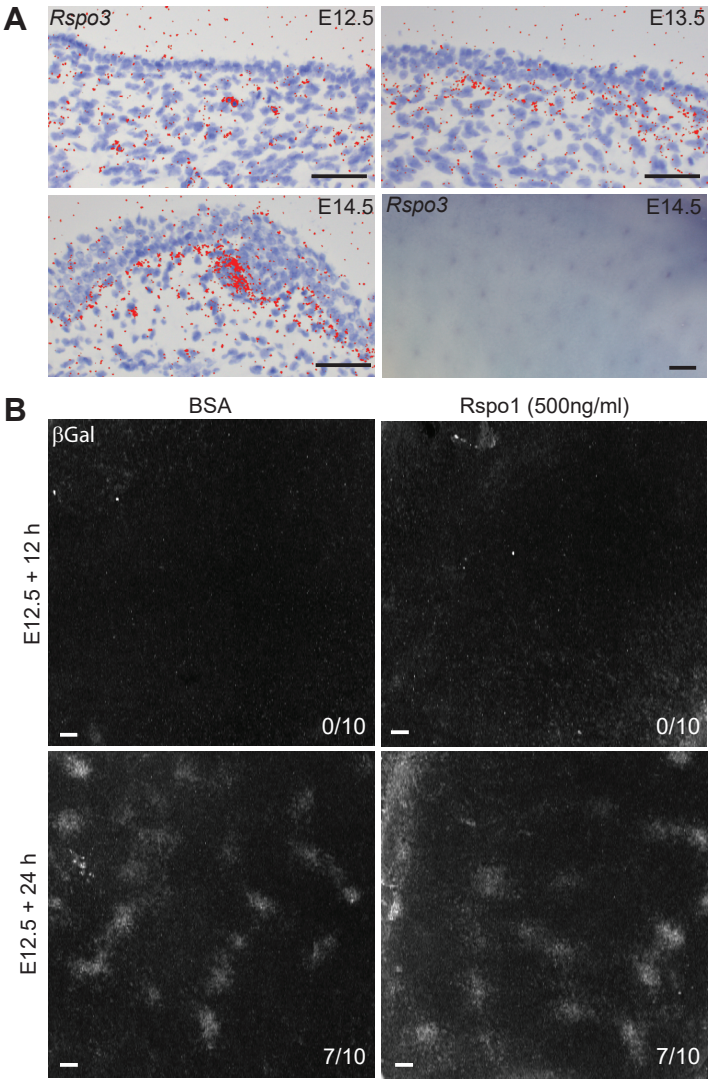

Fig S4 (Related to Fig. 6)**. *Rspo3* is expressed in dermal condensates.** (A) *Rspo3* expression in back skin of E12.5 (N=4), E13.5 (N=5), and E14.5 (N=5) wild type embryos, detected by RNA *in situ* hybridization. *Rspo3* whole mount *in situ* hybridization on E14.5 embryo (N=9). (B) Maximum intensity projection of confocal image stacks of BSA vehicle control and Rspo1 (500 ng/ml) treated Fgf20$^{\beta Gal/+}$ E12.5 back skin explants after 12 and 24 hours of culture with βGal immunolabelling. Numbers indicate samples with induced placodes / total number of samples. Scale = 50 µm, except wholemount ISH of *Rspo3* 200 µm.